Research Repository UCD

Title	Accuracy of instantaneous frequencies predicted by the Hilbert-Huang transform for a bridge subjected to a moving vehicle
Authors(s)	Casero, Miguel, González, Arturo, Covián, E.
Publication date	2020-07-02
Publication information	Casero, Miguel, Arturo González, and E. Covián. "Accuracy of Instantaneous Frequencies Predicted by the Hilbert-Huang Transform for a Bridge Subjected to a Moving Vehicle." CRC Press, July 2, 2020. https://doi.org/10.1201/9780429279119-220.
Conference details	The Tenth International Conference on Bridge Maintenance, Safety and Management (IABMAS 2020), Sapporo, Japan 28 June -2 July 2020
Publisher	CRC Press
Item record/more information	http://hdl.handle.net/10197/12145
Publisher's statement	This is an Accepted Manuscript of a book chapter published by CRC Press in Bridge Maintenance, Safety, Management, Life-Cycle Sustainability and Innovations: Proceedings of the Tenth International Conference on Bridge Maintenance, Safety and Management (IABMAS 2020) on 20 April 2021, available online: or http://www.crcpress.com/9780429279119
Publisher's version (DOI)	10.1201/9780429279119-220

Downloaded 2026-05-02 00:27:51

The UCD community has made this article openly available. Please share how this access benefits you. Your story matters! (@ucd_oa)

© Some rights reserved. For more information

Accuracy of instantaneous frequencies predicted by the Hilbert-Huang transform for a bridge subjected to a moving vehicle

M. Casero & A. González
University College Dublin, Dublin, Ireland

E. Covián
Universidad de Oviedo, Oviedo, Spain

ABSTRACT: This paper investigates the accuracy of the Hilbert-Huang transform (HHT) in capturing the time-varying frequencies of a short-span bridge traversed by a vehicle travelling at a constant speed. The bridge and vehicle are modelled as a simply supported beam and a quarter-car, respectively. The HHT uses empirical mode decomposition to divide the original signal into mono-component signals, called intrinsic mode functions (IMFs), where the Hilbert transform can extract instantaneous frequencies (IFs). Each IMF is associated with a dominant frequency band, although mode mixing is possible. In order to improve the predicted frequencies, several filters are applied before and after performing the HHT with a threefold purpose: (i) to remove the static component, (ii) to isolate the first mode of vibration, and (iii) to obtain meaningful and denoised IFs. The influences of a localized stiffness loss in the bridge, different vehicle speeds, and three signal-to-noise ratios on the results are discussed.

1 INTRODUCTION

The characterization of the dynamic properties of a bridge is of significant importance in the monitoring of structures. Changes in the natural frequencies and mode shapes (Kim et al. 2003) and damping ratios (Curadelli et al. 2008) of the structure are often used as damage detection methods. In order to obtain the mode shapes of a structure, it is necessary to place several sensors along the structure; however, one or two sensors are usually enough to capture the natural frequencies (Carden & Fanning 2004). Operational modal analysis aims to obtain the dynamic properties of the structures under its operational loading, i.e. when traffic is traversing a bridge.

Vehicle-bridge interaction (VBI) models serve to analyze how the presence of a vehicle affects the dynamic properties of the bridge. Generally, vehicles are modelled as a combination of masses that interact with each other and with the bridge via springs. The mass and stiffness properties of the VBI model combining the vehicle and the bridge differ from those properties of the bridge alone. Therefore, the VBI model leads to a variation of the frequencies of vibration of the bridge while traversed by the vehicle as demonstrated by Yang et al. (2013), Chang et al. (2014), González et al. (2015) and González et al. (2020) using eigenvalue analysis. Both Yang et al. (2013) and Chang et al. (2014) model the vehicle as a sprung mass and derive analytical expressions that relate the frequency of the bridge in forced vibration to the original frequencies of bridge and vehicle. On the other hand, González et al. (2015) conduct analyses on a 3D model using a 5-axle truck and González et al. (2020) investigate the impact that the presence of damage has on the forced frequencies of the bridge.

When using field measurements, the mass and stiffness matrixes will not be available, and it becomes necessary to employ a signal processing tool in the time-frequency domain that will characterize the time-varying frequencies of the system. Some of the most popular signal processing tools are the Short-time Fourier Transform (STFT), Continuous Wavelet Transform (CWT) and Hilbert-Huang Transform (HHT). The STFT is an extension of the FFT that uses a moving window to obtain instantaneous frequencies and to achieve a time-frequency domain representation. However, the selection of the window size may be challenging, since it leads to a trade-off between the time and frequency resolutions (Amezquita-Sánchez & Adeli 2016). The CWT is widely used due to its versatility and computational efficiency. Cantero & Obrien (2013) test several mother wavelets for the CWT on the simulated

response of a beam traversed by a sprung mass, to investigate the variation of the 1st natural frequency with the position of the vehicle. Their results indicate that the maximum variation of the frequency happens when the vehicle is located at midspan, which is the point of maximal modal amplitude for the 1st mode. They also find that the magnitude of the frequency variation is linked to the mass and frequency ratios between the sprung mass and the beam. Higher mass ratios and frequency ratios closer to one lead to more significant frequency variations. Lab experiments (Cantero et al. 2019) and field tests (Cantero et al. 2017) provide further experimental evidence on the variation of the forced frequency.

The STFT and CWT are very similar to each other, i.e., the signal is assumed to be stationary and a shape (sinusoidal in the case of STFT or mother wavelet in the case of CWT) is stretched and scaled to be compared to the original signal at each point in time in order to establish the frequency content. However, for a non-stationary signal, the instantaneous frequencies calculated by STFT and CWT may be smoother than in reality. In contrast, the HHT is conceptually different, given that it is built to deal with non-stationary signals. The HHT consists of two basic steps. In a first step, the signal is split into several Intrinsic Mode Functions (IMFs) through an iterative process using Empirical Mode Decomposition (EMD). IMFs are mono-component signals, which allows applying the Hilbert Transform (HT) to obtain the Instantaneous Frequencies (IFs) in a second step. González & Aied (2015) use the HHT to successfully identify damage in non-linear bearings by analyzing the IFs of the system.

One of the limitations of the HHT arises precisely from the incorrect separation of the signal components using EMD. Often, two IMFs that should correspond to two distinct modes with completely different frequencies may show interchanged frequencies. This phenomenon is called mode-mixing, and there are several variations of the EMD process in the literature that intend to mitigate its impact, such as Ensemble EMD (EEMD) (Torres et al. 2011), Complementary EEMD (Yeh et al. 2010) or Partly Ensemble EMD (Zheng et al. 2013). For instance, Aied et al. (2015) employ EEMD to characterize sudden stiffness changes of stiffness on a plate model when a 2-axle vehicle is driving over it.

This paper develops a strategy to improve the accuracy of the HHT in capturing the instantaneous 1st bridge frequency during forced vibration. Initially, two moving average filters (MAFs) are applied to the acceleration response from the bridge to identify its static component. Gonzalez & Hester (2013) use a similar approach of a double MAF to obtain the static component from an acceleration record for damage detection. This static component is later subtracted from the original response to obtain an estimation of the dynamic component. Then, a low-pass filter is applied to the dynamic component to remove the higher frequencies and to prevent mode-mixing when applying the HHT. Finally, a weighted average filter algorithm (WAFA) is used to smooth the calculated IFs. The concept is introduced using the theoretical response of a beam model due to a moving constant force and then tested using a coupled VBI model.

Section 2 describes the numerical models used for simulating the response of a bridge crossed by a vehicle. Section 3 shows how the combination of MAFs, low-pass filter and WAFA can contribute to improving the instantaneous frequencies predicted by the HHT in the case of a moving constant force crossing a bridge in healthy or damaged structural condition. Section 4 expands the analysis to a moving sprung vehicle interacting with the bridge, allowing for a range of speeds and signal to noise ratios. Finally, Section 5 outlines the conclusions and future lines of research drawn from this work.

2 VEHICLE-BRIDGE INTERACTION MODEL

Figure 1 shows the bridge and vehicle models used in the simulations. The bridge is modelled as a 15 m long simply supported beam discretized into 150 Euler-Bernoulli elements with two degrees of freedom (vertical displacement and rotation) at each node. The depth of the beam (d) is 0.6 m, leading to a moment of inertia per unit breadth of $0.6^3/12 = 0.018$ m^4/m. The properties of the material are representative of reinforced/prestressed concrete: Young's modulus of $35\text{x}10^6$ kN/m^2, Poisson's ratio of 0.15 and density of 2500 kg/m^3. The total mass of the bridge, assuming a width of 10 m, is 15x10x0.6x2500 = 225 tons. The first and second natural frequencies are 4.52 and 18.10 Hz, respectively. Bridge damping is typically low, and it is neglected in the analysis.

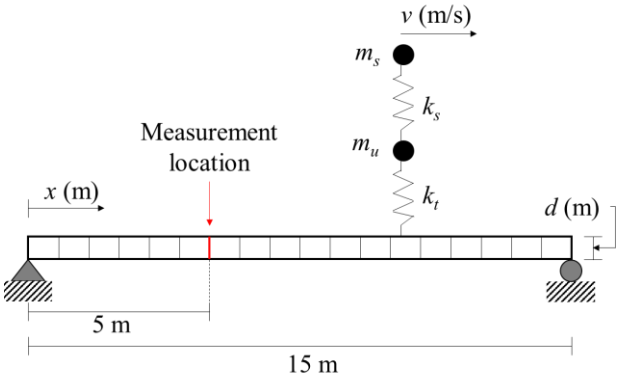

Figure 1. VBI model.

The vehicle is modelled using a quarter car, consisting of two masses connected to each other and to the bridge via springs. One degree of freedom is related to the upper mass (m_s), representing the body of the vehicle (m_s = 9300 kg), and another degree of

freedom is related to the lower mass (m_u), corresponding to the mass of an axle (m_u = 700 kg). The ratio of the vehicle mass to the bridge mass is 0.044. The top and bottom springs (k_s and k_t) represent the suspension (k_s = 1.8x10^3 kN/m), and the tire (k_t = 10^3 kN/m) respectively. The frequencies of the vehicle are 1.30 Hz (body bounce) and 10.22 Hz (axle hop). Vehicle damping is not considered here.

In Section 3, the interaction between the vehicle and the bridge is prevented. As a result, the analysis is similar to a moving point load with a constant magnitude equal to the total weight of the vehicle (i.e., 10 ton). In Section 4, the dynamic interaction between vehicle and bridge is allowed. The coupled equations of motion of vehicle and bridge are solved using the Wilson-Theta method (González 2010). The sampling frequency used in the simulations is 1000 Hz. Unless otherwise specified, the vehicle is assumed to move at a slow, constant speed of 1 m/s over the beam.

3 HHT OF THE BRIDGE RESPONSE DUE TO A MOVING POINT LOAD

3.1 *Healthy bridge*

Figure 2 shows the total acceleration response at x = 5 m from the left support of the bridge described in Section 2 due to a moving point load. The total acceleration in the figure can be divided into static (as a result of the static deflection of the bridge) and dynamic (as a result of the time-varying inertial forces of the vehicle and bridge) components.

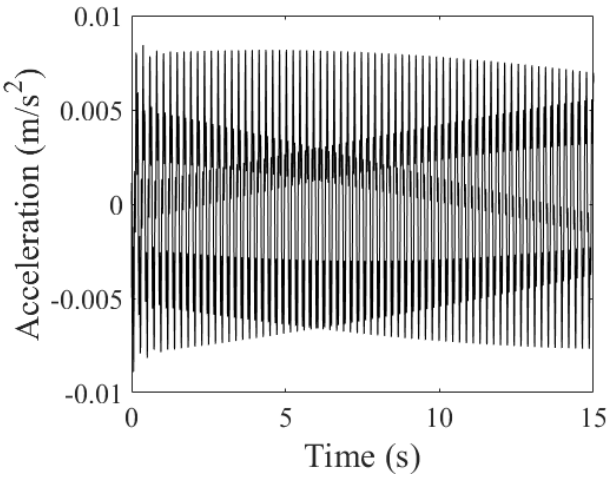

Figure 2. Simulated acceleration response of a bridge due to a moving point load.

This paper proposes a procedure to improve the accuracy of the frequencies predicted by the HHT. The methodology consists of three stages: (1) pre-processing of the original total acceleration to isolate the mode of vibration of interest before applying the HHT, (2) processing of the filtered acceleration by the HHT to obtain the IFs, and (3) post-processing of the IFs to remove noise.

In stage (1), the static component will be removed from the total response to extract the dynamic component as accurately as possible. For this purpose, a MAF is applied. Before applying the MAF, the response shown in Figure 2 is mirrored using anti-symmetric padding to mitigate edge effects (González et al. 2019). The span of the MAF is defined by a number of points in accordance with the first period of vibration of the bridge. Using the 1st natural frequency, which can be obtained from the free vibration of the bridge, the value of the first period of vibration is 0.221 s. Since the sampling frequency is 1000 Hz, the first period corresponds to 221 points in the simulated signal. For calculating the new value of each point in the filtered response, a total of 221 points are selected, with the point of interest being at the center of the set of points, and their values are added and divided by 221. The filtered response derived from applying the MAF is shown in Figure 3(a) using a solid blue line. The static component due to a moving load is expected to be triangular, with a maximum at the measurement location. An FFT of the filtered response provides evidence that the first frequency of the bridge has not been completely eliminated by applying the MAF. The power spectrum in Figure 3(b) indicates that although the dominant frequencies concentrate now around zero, there is still a small peak at around 4.5 Hz. A second peak can also be observed at around 18 Hz, corresponding to the 2nd bridge frequency. Thus, a second MAF with the same parameters as the previous MAF (221 points) is applied, obtaining the dashed red line in Figure 3(a). The remaining response does present a clear triangular shape. Even with the mirroring of the response, edge effects are unavoidable and will become more relevant as the speed of the vehicle increases.

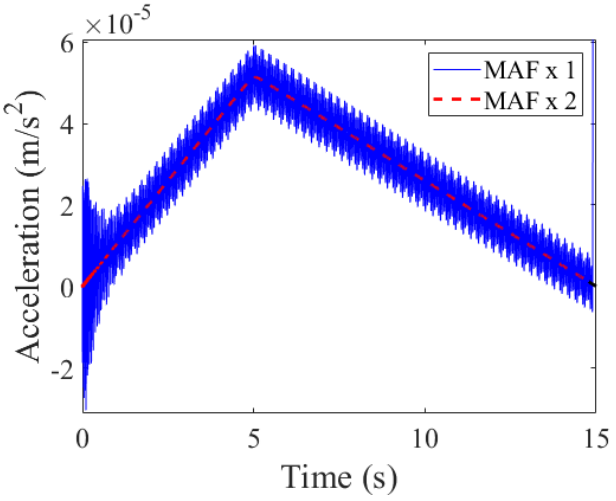

(a)

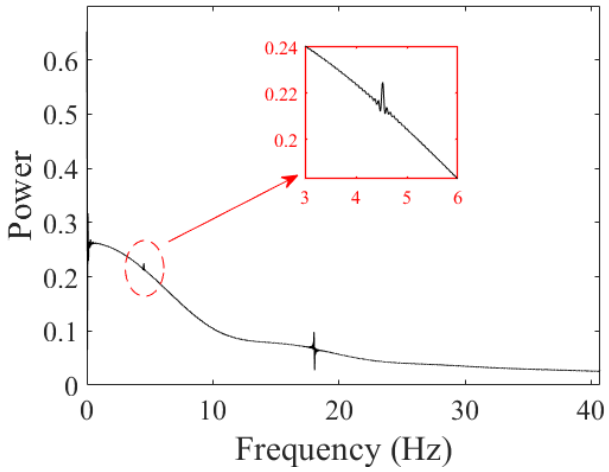

(b)

Figure 3. (a) Estimated static component of acceleration in Figure 2 using MAFs; and (b) Power spectrum of the response filtered using one MAF.

Once the static component of the response has been identified, it is subtracted from the original response in Figure 2, so that only an estimation of the dynamic component remains. Then, an eighth-order low-pass Butterworth filter with a cut-off frequency of 6 Hz is applied to the estimated dynamic component to eliminate high frequencies that are of no interest and a potential source of mode mixing.

In stage (2), EMD is applied to obtain the IMFs from the estimated dynamic component associated with the main mode of vibration. In order to mitigate the edge effects, the approach proposed by Wang & Ji (2018) is applied here. As part of the EMD process, the upper and lower envelopes of the signal must be calculated through spline interpolation. However, given the impossibility of calculating local minima or maxima at the ends of the signal, it is possible that the spline fitting results in large swings of the envelopes, i.e. the upper envelope crossing over the lower envelope. In order to avoid this problem, Wang & Ji propose a linear interpolation approach for the end of the signal based on the last two local minima or maxima. Finally, the HT is applied leading to the IFs in Figure 4(b). For comparison purposes, the HHT is also tested on the original response (Figure 4(a)). Given that there is no interaction taking place between vehicle and bridge, the 1st bridge frequency should remain invariable and it is represented by a horizontal dashed black line in Figure 4. The horizontal axis is given in terms of vehicle position on the bridge, *x*, with respect to the left support (Figure 1), to facilitate comparisons when the speed of the vehicle is modified in subsequent analyses.

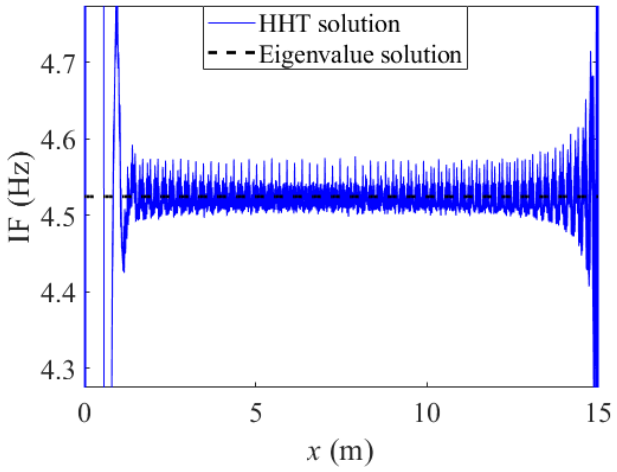

(a)

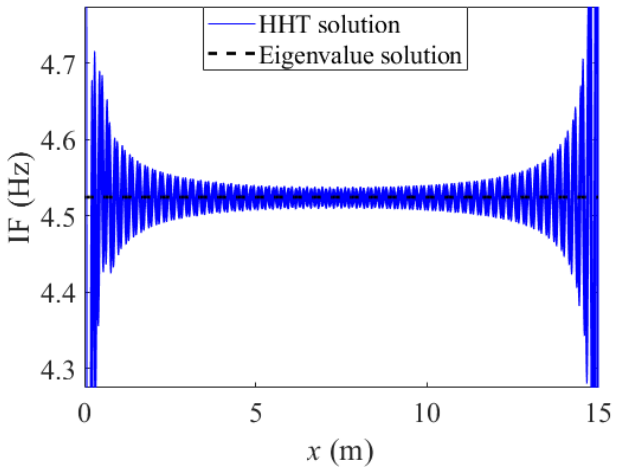

(b)

Figure 4. Instantaneous frequencies of the: (a) original response, and (b) dynamic component with a low-pass filter.

In stage (3), the results from Figure 4 are further improved by applying a WAFA to the IFs as recommended by Niu et al. (2012). Equation 1 defines the amplitudes associated with each IF as the weights to compute a weighted average of each IF over a number of points.

$$\overline{IF(k)} = \begin{cases} \dfrac{\sum_{j=1}^{k+(m-1)/2} IF(k)\cdot A(k)}{\sum_{j=1}^{k+(m-1)/2} A(k)} & j\epsilon[1,(m-1)/2] \\ \dfrac{\sum_{j=k-(m-1)/2}^{k+(m+1)/2} IF(k)\cdot A(k)}{\sum_{j=k-(m-1)/2}^{k+(m+1)/2} A(k)} & j\epsilon[(m+1)/2\,,(2N-1-m)/2] \\ \dfrac{\sum_{j=k-(m-1)/2}^{N} IF(k)\cdot A(k)}{\sum_{j=k-(m-1)/2}^{N} A(k)} & j\epsilon[(2N+1-m)/2\,,N] \end{cases} \quad (1)$$

where $\overline{IF(k)}$ = weighted average value of $IF(k)$; k = index of IF being averaged; $A(k)$ = amplitude associated to $IF(k)$; m = maximum number of IFs used to calculate the weighted average value; and N = total number of IFs.

It must be noted that $\overline{IF(k)}$ is a piecewise function. When k represents an IF close to the edge, the number of points between the beginning/end of the signal and

the index k is less than half the value of m minus one. In those cases, the weighted average is computed using a number of points smaller than m, as reflected by the first and third sub-functions in Equation (1). For instance, if k = 1, the weighted average is computed based only on $IF(1)$ and the next (m-1)/2 points, i.e. a total of m/2 points.

As was the case with the MAF applied to obtain the static component, the selection of the window length is an important parameter here. A window size of m = 225 samples is chosen based on the expected frequency. The resulting IFs are shown in Figure 5, with the horizontal dashed line representing the 1st frequency.

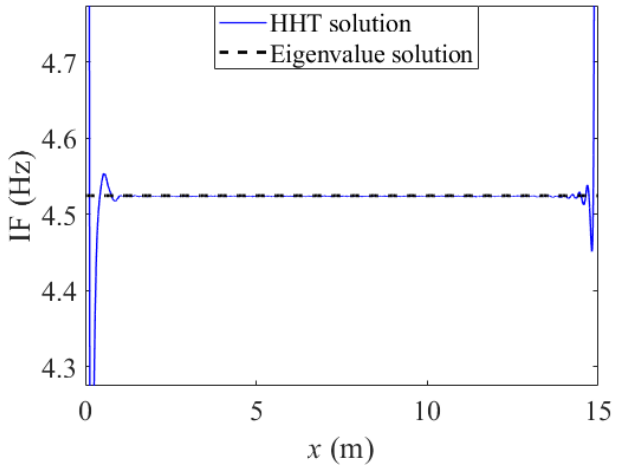

Figure 5. Instantaneous frequencies after applying WAFA to the IFs in Figure 4(b).

Table 1 contains the root mean square errors (RMSE) of the predicted IFs for three segments of the bridge span. RMSE is calculated as per Equation 2.

$$RMSE = \sqrt{\sum_{k=1}^{n} \frac{\left(IF(k)_{eig} - IF(k)\right)^2}{n}} \quad (2)$$

where $IF(k)_{eig}$ = frequency obtained from eigenvalue analysis; and n = number of points over which RMSE is calculated.

In this case, the subtraction of the static component does not have a significant effect on accuracy, but the application of the low-pass filter considerably reduces the error in the predicted frequency. This is especially noticeable near the left support where the edge effects have a significant effect on the non-filtered responses. When applying WAFA in post-processing of the dynamic filtered, edge effects are still present and remain a challenge, but the prediction of the frequency is highly accurate in the central part of the bridge. Edge effects may be reduced to some extent by further increasing the window length of the WAFA but at the cost of losing accuracy in the central part of the bridge.

Table 1. RMSE (Hz) of the predicted frequencies without interaction between bridge and vehicle.

Response	0 - 15 m	3 - 12 m	6 - 9 m
Original	2.415	0.014	0.014
Dynamic	2.415	0.014	0.014
Dynamic filtered	0.809	0.011	0.009
Dynamic filtered +WAFA	0.242	0.001	0.001

3.2 *Damaged bridge*

The stiffness loss due to a crack is modelled following Sinha et al. (2002), who assume that there is a linear variation of stiffness from the location of the crack (maximal stiffness loss) to a distance equal to 1.5d at both sides of the crack (zero stiffness loss), where d represents the depth of the beam. A crack with a depth equal to 0.12 m is adopted. The crack is located at x = 9 m, thus elements between x = 8.1 m and x = 9.9 m are affected by the crack

The same methodology as before is then repeated for the acceleration response of the vehicle passing over the damaged bridge. The static component is subtracted from the total response and higher frequency components are removed using a low-pass filter with a cut-off frequency of 6 Hz. Figure 6 shows the IFs that are obtained following the application of the WAFA, together with the IFs corresponding to the healthy bridge. The first frequencies of vibration of the healthy and damaged bridges are represented by horizontal dashed and dotted lines respectively.

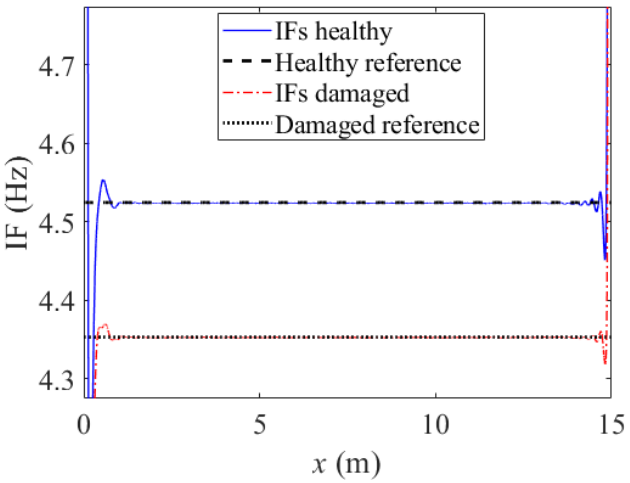

Figure 6. Comparison of instantaneous frequencies associated with healthy and damaged bridges.

It can be seen that the HHT is able to capture the permanent change in frequency due to the presence of damage as the IFs oscillate now around the new 1st bridge frequency (4.35 Hz). The difference in first frequencies of vibration between damaged and healthy bridges is 0.17 Hz, i.e., a 3.79% decrease. A more challenging scenario is presented in Section 4 when the HHT is used to capture the slight and

gradual variations of frequency caused by the movement of a vehicle along the bridge.

4 HHT OF THE BRIDGE RESPONSE DUE TO A QUARTER-CAR MODEL

In the previous section, the moving point load model neglects the interaction between the vehicle and the bridge. Hence there is no possible variation in the 1st frequency of the bridge. If the simulations were repeated using the sprung vehicle model of Section 2, a variation in the predicted IFs could be expected. The evolution of the frequency of the bridge with the position of the vehicle can be obtained from the eigenvalue analysis of the VBI model. For each potential location of the vehicle, the varying global stiffness matrix can be computed and, together with the global mass matrix, allow obtaining the frequency of the system associated with the 1st mode of vibration of the bridge. Figure 7 shows both the frequency values obtained from eigenvalue analysis (dashed line) and the IFs (continuous line) obtained from applying the three-stage HHT procedure described in Section 3.1 to the acceleration response due to the quarter-car. There is a difference of 0.016 Hz between the maximum eigen-frequency and the 1st bridge frequency in free vibration, which represents a maximum change in forced frequency of only 0.35% that is challenging to capture.

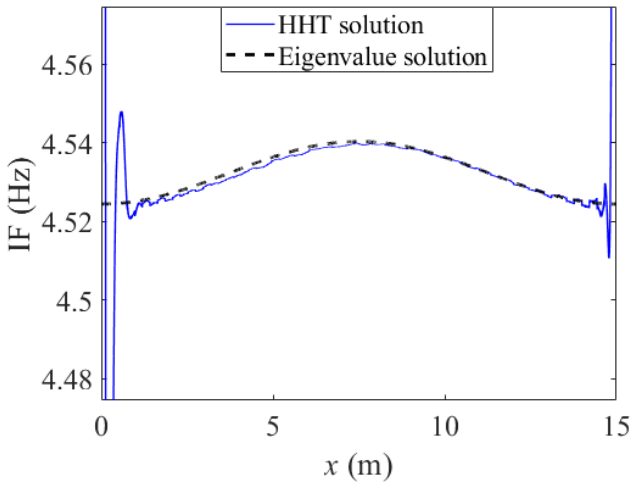

Figure 7. Instantaneous forced frequencies from coupled VBI system due to a vehicle travelling at 1 m/s.

As reported in the literature, the IFs in forced vibration have a gradual evolution, leading to a maximal variation with respect to the 1st bridge frequency when the vehicle is located at midspan. Both the eigen-frequencies and the IFs resemble this pattern in Figure 7. Edge effects arising from the application of the HHT lead to a poor prediction of frequencies in the intervals $x \in [0,1]$ and $x \in [14,15]$. Nonetheless, the RMSE for frequencies between x = 1 m and x = 14 m is 0.001 Hz.

4.1 *Impact of vehicle speed*

The speed of the vehicle has been kept at a low value (1 m/s) to obtain a long response that is beneficial towards predicting frequencies with high-resolution. In this section, speed is gradually increased to test the accuracy of the HHT with shorter responses. Figure 8 shows the instantaneous frequencies obtained for speeds of 2 m/s, 4 m/s, 6 m/s and 8 m/s. The frequencies from the eigenvalue analysis are also shown as a thick dashed black line for reference purposes. It can be seen how a higher speed amplifies the negative edge effects and causes a loss of accuracy in the predicted frequencies. The most inaccurate results are obtained for 8 m/s, when the response in forced vibration is only 1.875 s long.

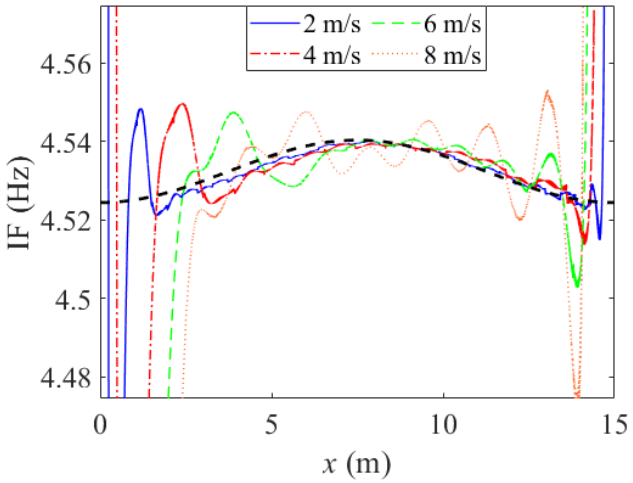

Figure 8. Instantaneous forced frequencies from coupled VBI system due to vehicle travelling at 2, 4, 6 and 8 m/s.

In spite of the inaccuracies near the supports, Table 2 shows that the RMSE is kept at reasonable low values for the central segment of the bridge, i.e., between x = 6 and x = 9 m.

Table 2. RMSE (Hz) of the predicted frequencies for the coupled VBI system using different speeds of the quarter-car.

Speed	0 - 15 m	3 - 12 m	6 - 9 m
1 m/s	0.164	0.001	0.001
2 m/s	0.180	0.001	0.001
4 m/s	0.251	0.003	0.001
6 m/s	0.272	0.006	0.003
8 m/s	0.605	0.006	0.005

4.2 *Impact of noise*

An additive Gaussian noise model is used to contaminate the acceleration response with low, moderate

and high noise levels. The level of noise is characterized by the signal-to-noise ratio (SNR), which is defined as the ratio of the standard deviation of the clean acceleration response (σ_S) to the standard deviation of the noise (σ_N). Therefore, a high value of SNR implies a low amount of noise and vice-versa. Equation 3 is used to simulate a measured signal by adding noise to the theoretical response.

$$\{a_N\} = \{a_s\} + \sigma_N \cdot \{N(0,1)\} = \{a_s\} + \frac{\sigma_s}{\text{SNR}} \cdot \{N(0,1)\} \qquad (3)$$

where $\{a_N\}$ = vector containing the noisy acceleration, $\{a_s\}$= vector containing the theoretical acceleration response; and $\{N(0,1)\}$ = vector containing values randomly sampled from a standard normal distribution with zero mean and unit standard deviation.

Figure 9 shows the IFs obtained from applying the HHT to the theoretical response at 1 m/s corrupted with SNRs of 20, 10 and 5, representing relative errors in the measurements of 5%, 10% and 20% respectively. Although the prediction of the frequency becomes more inaccurate as noise increases, the method proves to be quite robust, even for relatively high levels of noise.

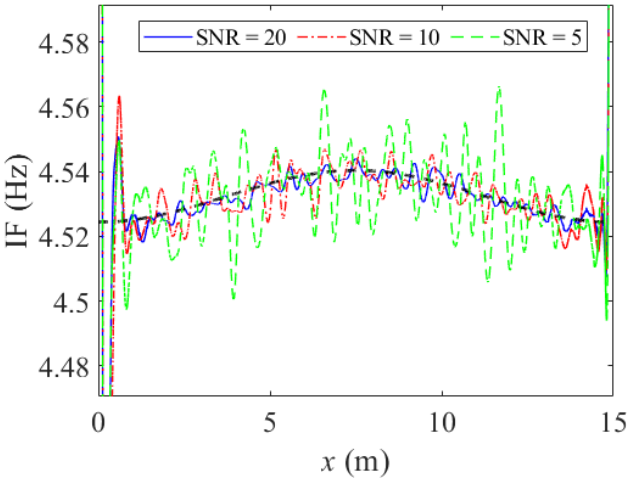

Figure 9. Instantaneous forced frequencies from the response of a coupled VBI system due to vehicle travelling at 1 m/s, corrupted with three signal-to-noise ratios.

Table 3 summarizes the RMSEs for each level of noise. The random nature of noise leads to a surprisingly lower RMSE for the moderate level of noise (SNR = 10) when considering the whole length of the bridge, i.e. including areas close to the supports.

Table 3. RMSE (Hz) of the predicted frequencies for different levels of noise.

SNR	0 - 15 m	3 - 12 m	6 - 9 m
Noise-free	0.164	0.001	0.001
20	0.163	0.002	0.002
10	0.094	0.005	0.005
5	0.164	0.013	0.012

5 CONCLUSIONS

A methodology has been proposed to improve the accuracy of the HHT in estimating the 1st frequency of a short-span bridge in forced vibration. Prior to the implementation of the HHT, a moving average filter has been used to extract the static component from the original response. The static component has been subtracted from the original response to obtain the dynamic component of the response. A low-pass filter has then served to remove frequency components above the 1st bridge frequency. Finally, the accuracy of the IFs by the HTT associated with this low-frequency dynamic component has been enhanced via a weighted average frequency algorithm.

The HHT, in combination with the filters proposed above, has been able to quantify the change in forced frequency due to a localized stiffness loss. When the interaction between the bridge and a moving vehicle was allowed, the methodology has accurately captured the small changes in the forced frequency of the bridge derived from the different positions of the vehicle, except near the supports. Edge effects make unfeasible the accurate prediction of frequencies near the supports and its negative influence has grown more significant as the response became shorter. As a result, an increase in speed has shortened the portion of the bridge over which the HHT is able to provide reliable values of IFs. In the central portion of the bridge and away from the supports (i.e., from 1/5 to 4/5 of the span), the methodology has dealt with low to moderate levels of noise successfully. Future research is needed to improve the prediction of frequencies for locations of the vehicle near the supports and higher speeds of the vehicle.

ACKNOWLEDGEMENTS

This research has received funding from Science Foundation Ireland (SFI)'s US-Ireland R&D partnership programme under the proposal id. 16/US/I3277 titled MARS-Fly.

REFERENCES

Aied, H., González A. & Cantero, D. 2015. Identification of sudden stiffness changes in the acceleration response of a bridge to moving loads using ensemble empirical mode decomposition. *Mechanical Systems and Signal Processing* 66-67: 314–338.

Amezquita-Sanchez, J.P. & Adeli, H. 2016. Signal processing techniques for vibration-based health monitoring of smart structures. *Archives of Computational Methods in Engineering* 23(1): 1-15.

Cantero, D. & OBrien, E.J. 2013. The non-stationarity of apparent bridge natural frequencies during vehicle crossing events. *FME transactions* 41(4): 279-284.

Cantero, D., Hester, D. & Brownjohn, J. 2017. Evolution of bridge frequencies and modes of vibration during truck passage. *Engineering Structures* 152: 452-464.

Cantero, D., McGetrick, P., Kim, C. W. & OBrien, E. 2019. Experimental monitoring of bridge frequency evolution during the passage of vehicles with different suspension properties. *Engineering Structures* 187: 209-219.

Carden, P. & Fanning, P. 2004. Vibration based condition monitoring: A review. *Structural Health Monitoring* 3(4): 355-377.

Chang, K.C., Kim, C.W. & Borjigin, S. 2014. Variability in bridge frequency induced by a parked vehicle. *Smart Structures and Systems* 13(5): 755-773.

Curadelli, R. O., Riera, J. D., Ambrosini, D. & Amani, M.G. Damage detection by means of structural damping identification. *Engineering Structures* 30(12): 3497-3504.

González, A. 2010. Chapter 26: Vehicle-bridge dynamic interaction using finite element modelling. In D. Moratal (eds), *Finite Element Analysis*: 637-662. Croatia: InTech.

González, A. & Hester, D. 2013. An investigation into the acceleration response of a damaged beam-type structure to a moving force. *Journal of Sound and Vibration* 332 (13): 3201-3217.

González, A. & Aied, H. 2015. Characterization of non-linear bearings using the Hilbert–Huang transform. *Advances in Mechanical Engineering* 1-13.

González, A., Covián, E. & Casero, M. 2015. Impact of superimposed and truck live load on modal characteristics of short-span bridges. 6th *International Modal Analysis Conference (IOMAC)*.

González, A., Feng, K. & Casero, M. 2019. Numerical analysis of techniques to extract bridge dynamic features from short records of acceleration. *IABSE Symposium Guimarães* 2019 *Towards a Resilient Built Environment Risk and Asset Management*.

González, A., Casero, M. & Feng, K. 2020. Sensitivity to Damage of the Forced Frequencies of a Simply Supported Beam Subjected to a Moving Quarter-Car. *Lecture Notes in Mechanical Engineering*: 350-362.

Kim J. T., Ryu, Y. S., Cho, H. M. & Stubbs, N. 2003. Damage identification in beam-type structures: frequency-based method vs mode-shape-based method. *Engineering Structures* 25(1): 57-67.

Niu, J., Liu, Y., Jiang, W., Li, X. & Kuang, G. 2012. Weighted average frequency algorithm for Hilbert–Huang spectrum and its application to micro-Doppler estimation. *IET Radar, Sonar and Navigation* 6(7): 595-602.

Sinha, J. K., Friswell, M. & Edwards, S. 2002. Simplified models for the location of cracks in beam structures using measured vibration data. *Journal of Sound and vibration* 251(1): 13-38.

Torres, M. E., Colominas, M. A., Schlotthauer, G. & Flandrin, P. 2011. A complete Ensemble Empirical Mode decomposition with adaptive noise. *IEEE Int. Conf. on Acoustic, Speech and Signal Processing (ICASSP)*.

Wang, H. & Ji, Y. 2018. A revised Hilbert–Huang transform and its application to fault diagnosis in a rotor system. *Sensors* 18(12): 4329.

Yang, Y. B., Cheng, M. C. & Chang, K. C. 2013. Frequency variation in vehicle bridge interaction systems. *International Journal of Structural Stability and Dynamics* 13(2): 1-22.

Yeh, J. R., Shieh, J. S. & Huang, N. E. 2010. Complementary ensemble empirical mode decomposition: a novel noise enhanced data analysis method. *Advances in Adaptive Data Analysis* 2(2): 135-156.

Zheng, J., Cheng, J. & Yang, Y. 2014. Partly ensemble empirical mode decomposition: An improved noise-assisted method for eliminating mode mixing. *Signal Processing* 96: 362–374.